PAPER

Check for updates

Matrinium-based active pharmaceutical ingredient ionic liquids: chain length effect on micellization, bioactivity and thermodynamic behaviors†

Zhenning Yan, [iD] * Mengmeng Xu and Huanhuan Lu

The active pharmaceutical ingredient ionic liquids (API-ILs) obtained from bio-renewable and natural compounds are noted for their good safety and biodegradability. This study focused on the utilization of naturally occurring matrine (Mat) in the synthesis of matrinium-based API-ILs with attractive application potential. Five matrinium-based API-ILs were synthesized by a neutralization reaction between Mat and biodegradable saturated fatty acids (enanthic acid, pelargonic acid, undecanoic acid, tridecanoic acid, and pentadecanoic acid). We typically employed ^{1}H and ^{13}C NMR, FTIR, ESI-MS, and thermogravimetric analysis techniques for characterization of the structural properties of the synthetic API-ILs. Additionally, the *n*-octanol–water partition coefficient as well as the solubility of these ILs in various mediums were measured. The solvation behavior, association, and aggregation properties were studied through density, conductivity, and fluorescence spectrometry analyses, respectively. Many parameters such as apparent molar volume at infinite dilution ($V_{2,\varphi}^0$), limiting molar conductivity (Λ_0) and critical micelle concentration (cmc) of MatILs in water, association constant (K_A), and related micellization thermodynamic functions were calculated. The minimum inhibitory concentrations (MICs) of three API-ILs against four strains (*Escherichia coli*, *Staphylococcus aureus*, *Candida albicans*, and *Cutibacterium acnes*) were determined. The results demonstrated their potent antibacterial efficacy. Through cytotoxicity assays, it was observed that compared to Mat, the synthesized API-ILs exhibited enhanced cytotoxic effects on two human tumor cell lines (A549 and HepG2). Furthermore, we systematically correlated anion alkyl chain length with some of the physicochemical properties and biological activities of ionic liquids to elucidate structure–property relationships.

1. Introduction

In recent years, the use of active pharmaceutical ingredient ionic liquids (API-ILs) has dramatically escalated in the fields of pharmaceutics and medicine because they allow solid active pharmaceutical ingredients (APIs) to undergo fine modulation of their physical and chemical properties, such as higher solubility, thermal stability, dissolution, permeability, and the elimination of polymorphisms and cytotoxicity on tumor cells.[1] Because of the recent concerns regarding safety after the biodegradation of drugs, the synthesis of API-ILs using renewable and nontoxic natural sources is growing.

The cholinium-based API-ILs are one of the most studied classes. Choline chloride is a vitamin B drug that can form API-ILs with different active compounds, such as phenytoin,[2] methotrexate,[3] nalidixic acid, niflumic acid, 4-aminosalicylic acid, pyridine acid, and picolinic acid.[4] These API-ILs improve

the solubility of APIs and increase their capacity to pierce cell membranes, thus opening up the possibility of developing new or improved therapeutic platforms.

Amino acids, glucose, non-nutritive sweeteners, and carboxylic acids are commonly used to synthesize API-ILs.[5] Several studies have confirmed their improved benign character when compared with commonly used ILs.[5–7] Apart from the well-studied API-ILs mentioned above, those derived from naturally occurring and low-cost alkaloids are promising, but currently not a fully developed alternative for new API-ILs.

Matrine is a tetracyclic quinoline alkaloid derived from the roots of *Sophora flavescens*, and has demonstrated pharmacological activities, incorporating anti-tumor, antiviral, antimicrobial, and analgesic effects.[8] Matrine and its derivants have been widely utilized in conventional Chinese medicine for the treatment of various diseases. However, their application is limited due to factors such as restricted thermal stability, poor bioavailability, and relatively singular activity.[9]

The combination of matrine as a cation with a specific counter-ion is an excellent method to improve traditional pharmaceuticals. The long-chain fatty acid is a good choice because it is a facilitator of hydrophobic drug transport in the

College of Chemistry, Zhengzhou University, Zhengzhou, Henan 450001, P. R. China. E-mail: yanzzn@zzu.edu.cn

human body, and long-chain carboxylic acid ILs are also weakly polar, strongly hydrogen-bonded alkaline, and lipophilic, as well as water-soluble. Previous studies[10,11] reported good biodegradability in relation to long and unbranched alkyl side chains. It has been indicated that ILs with long alkyl side chains are more easily biodegraded and exhibit strong antibacterial activity and cytotoxicity.[12,13] Therefore, in the present study, we selected matrine as a cation, and long-chain fatty acids extracted from vegetable oil as anions to produce a series of matrinium-based ILs (MatILs).

The chosen five long-chain fatty acids are enanthic acid ($C_6H_{13}COOH$), pelargonic acid ($C_8H_{17}COOH$), undecanoic acid ($C_{10}H_{21}COOH$), tridecanoic acid ($C_{12}H_{25}COOH$), and pentadecanoic acid ($C_{14}H_{29}COOH$). The resultant substances are represented by the following symbols: $[Mat][C_7]$, $[Mat][C_9]$, $[Mat][C_{11}]$, $[Mat][C_{13}]$, and $[Mat][C_{15}]$, respectively. The five synthesized MatILs are protic ionic liquids (PILs) that possess the characteristics of low cost, easy synthesis, low toxicity, and high biodegradability.[14] Greaves and Drummond reviewed the properties and applications of pharmaceutical active protic ionic liquids and noted that some PILs exhibited good anti-inflammatory and antipyretic activity, and inhibitory effects on clot formation.[15]

Because a grasp of the basic physiochemical properties of a drug is imperative to comprehend its activity and functional mechanisms,[16] the present work focuses on the partition coefficient, solubility, thermal stability, solvation, and association and aggregation behaviors of synthetic MatILs. These properties can influence the solubility, stability, release characteristics, and toxicity of drugs. The data describing their bioactivity (antibacterial activity and cytotoxicity) are also presented.

As a structural parameter of a substance, the length of alkyl chains is an important factor influencing the properties and biological efficacy of ionic liquids.[17] Therefore, a systematic study was conducted on the influence of the anion alkyl chain length on the properties under investigation, and correlations between them were established. The effect of external environmental factors such as temperature and pH value on the properties was also explored.

2. Experimental

2.1. Chemicals

Matrine (99.0% purity) and all used fatty acids (98% purity) were obtained from Macklin Reagent Company (Shanghai, China). The organic solvents used in the study were purchased from Sinopharm Chemical Reagent Co., Ltd (Shanghai, China), including octanol (99.0%), ethanol (≥99.7%), methanol (≥99.5%), dichloromethane (≥99.5%), petroleum ether (≥99.5%), ethyl acetate (≥99.5%), acetonitrile (≥99.0%), toluene (≥99.0%), and acetone (≥99.0%). Cetylpyridinium chloride (≥98%) and pyrene (≥99%) were purchased from Sigma-Aldrich Shanghai Trading Co., Ltd. Potassium chloride (>99.999%; Aldrich Chemical Co.) was dried at 373 K for 48 h and used to calibrate the conductivity meter. Solutions were prepared using double-distilled deionized water (specific conductivity = $0.8 - 1.0 \times 10^{-4}$ S m^{-1} at 298.15 K).

Microorganisms *Staphylococcus aureus* ATCC29213, *Escherichia coli* ATCC25922, *Candida albicans* ATCC10231, and *Cutibacterium acnes* ATCC6919 were supplied by the American Type Culture Collection (ATCC). Two cell lines (human hepatocellular carcinoma cell line HepG2 and human lung cancer cell line A549) were purchased from Procell Biosciences, Inc. (Wuhan, China).

2.2. Synthesis of MatILs

Briefly, a solution of matrine (20 mmol) in 80 mL of ethanol was slowly added to 40 mL of ethanol solution of fatty acid (20 mmol), followed by stirring at room temperature for 8 h to ensure a complete reaction. The mixture for preparing $[Mat][C_{15}]$ was stirred at 40 °C, the ethanol was subsequently removed with a rotary evaporator, and the mixture was then dried in a vacuum drying oven for at least 48 h. Finally, a light yellow transparent liquid was obtained.

2.3. Characterization

The NMR spectra of MatILs were recorded on a Bruker DPX instrument with CDCl$_3$ as the solvent at 600 MHz for ^{1}H and 151 MHz for ^{13}C. All chemical shifts are quoted in ppm relative to TMS as an internal standard. Based on ^{1}H NMR data, the purity of the five MatILs was calculated from the ratio of the sum of the relative area of each NMR signal of the resulting compound to the sum of all signal areas,[18] and was found to be ≥97.0%.

The FT-IR spectra were measured in attenuated total reflection mode by means of KBr pellet using a Thermo Nicolet Nexus 470 (USA) FT-IR spectrometer equipped with a deuterated triglycine sulfate (DTGS) detector. The spectra were recorded in the frequency region of 400–4000 cm^{-1} under a resolution of 4 cm^{-1}, and with an accumulation of 20 scans.

Mass spectra measurements were acquired by direct infusion electrospray ionization mass spectrometry using an Agilent Triple quadrupole 6420 apparatus (LC/MS-MS) (USA). Molecular ions were analyzed in positive and negative mode.

Thermal stability measurements were carried out using a STA 449 F3 simultaneous thermal analyzer (Germany) in the range of 30–500 °C with a heating rate of 10 K min^{-1}. Approximately 3–5 mg of ILs was weighed in an Al$_2$O$_3$ crucible, and α-Al$_2$O$_3$ was used as the reference. Argon at a flow rate of 20 mL min^{-1} was used as a protective gas, and an argon atmosphere at a flow rate of 60 mL min^{-1} was used as a purge gas.

A differential scanning calorimetry (DSC) experiment was performed using a TA Q2000 calorimeter under nitrogen flow. The samples (2–5 mg) were sealed in aluminum pans, and before analysis, MatILs were dried at 120 °C for 30 min to remove possible volatile substances. The heating and cooling rates of 10 K min^{-1} and the temperature range of −80–100 °C were applied. Two heating and cooling cycles were used for each IL.

2.4. Solubility

Except for $[Mat][C_{15}]$, satisfactory aqueous solubility was exhibited for all other substances. The aqueous solubility of $[Mat][C_{15}]$ was determined at 25 and 37 °C. Simulated gastric fluid (SGF), simulated intestinal fluid (SIF), ultrapure water, and

simulated body fluid (SBF) were used as dissolution media with pH values of 1.2, 6.8, 7.0, and 7.4, respectively. Three simulated physiological fluids (without enzyme) were prepared according to the description by the United States Pharmacopeia. Excess [Mat][C_{15}] was added to the dissolution medium. The saturated solution was stirred in a water bath for 24 hours until it reached equilibrium. The supernatant was collected and filtered through a 0.46 μm syringe filter. Subsequently, the resulting filtrate was diluted with the corresponding dissolution medium. The absorbance of [Mat][C_{15}] at its maximum absorbance wavelength of 200 nm was measured using an ultraviolet (UV)-visible spectrometer (UV-1800PC, PerkinElmer), and the solubility was calculated according to a predetermined standard curve. Three replicates were performed for each solution.

The solubility of MatILs in organic solvents was tested with a commonly used solubility scheme.[19] Seven organic reagents were selected according to Snyder's polarity index values and sorted by polarity (methanol 6.6; acetonitrile 6.2; acetone 5.4; ethyl acetate 4.3; dichloromethane 3.4; toluene 2.3, and petroleum ether 0.0). A certain mass of MatILs (0.1 ± 0.0001 g) was placed in a graduated test tube and heated at 25 °C for dissolution. The amount of solvent added was 1, 2, 3 mL, and more than 3 mL, and the dissolution was then observed. According to the dosage of solvent, four behaviors of high solubility, medium solubility, low solubility, and insolubility were recorded.

2.5. Octanol–water partition coefficient

The partition coefficient of the MatILs was determined using the shake-flask method[20] at 25 and 37 °C. Three simulated physiological fluids mentioned above and ultra-pure water were used as solvents. First, a certain amount of water or buffer solution was mixed with n-octanol, violently oscillated at 25 and 37 °C for 24 h, and then maintained for 24 h for phase separation. MatIL solutions with different concentrations were prepared by dissolving a certain mass of ILs in 20 mL of water/buffer-saturated octanol. Next, 5 mL MatILs solution was appended to 5 mL octanol-saturated water/buffer solution, and the resultant solution was shaken for 24 h. The mixture was then centrifuged for 10 min. The octanol layer was extracted with a syringe. A UV-1800PC UV-Vis spectrophotometer was employed to determine the concentration (C_0) of MatILs in the equilibrium octanol phase at 200 nm. The octanol–water partition coefficient was calculated as follows:

$$\log K_{o/w} = \log C_o/(C - C_0) \tag{1}$$

where C represents the initial concentration in water/buffer solution-saturated octanol.

2.6. Conductivity measurement

A digital conductivity meter (model DDSJ-318, Shanghai Leici Company) and DJS-1D electrode were employed to measure the conductivity of MatIL solutions at different temperatures. The conductivity cell was calibrated with a standard KCl solution. The relative standard uncertainty for conductivity was ±3%. The temperature was controlled by a thermostat (DC-0506,

Shanghai Hengping Instrument Factory) with an accuracy of ±0.02 K.

2.7. Fluorescence measurement

Fluorescence spectra measurements were performed using an F4600 Shimadzu fluorescence spectrometer with a 150 W xenon lamp and 1 cm quartz cuvette. The experimental conditions were excitation wavelength of 335 nm, emission wavelength range of 355–650 nm, excitation and emission slit widths of 2.5 nm, voltage of 700 V, and scanning speed of 240 nm min^{-1}. Pyrene (1 μM) was used as a fluorescent probe. The ratio of the first (373 nm) over the third (384 nm) vibronic peak of pyrene fluorescence, I_1/I_3, was utilized to calculate the cmc values of the MatILs. The aggregation number of MatILs was estimated by measuring the intensities of the first peak of pyrene in the presence of the quencher (cetylpyridinium chloride) with the different concentrations, which slightly changed to ensure the Poisson distribution of the quencher.

2.8. Density measurement

The density of the solution was measured with a DMA 4500 M Anton Paar automatic vibrating tube digital densitometer (Austria). Before the testing, the density meter was calibrated with dry air and double-distilled water. The precision of the densitometer is ±0.00005 g cm^{-3}. The temperature was automatically controlled at ±0.01 K with a Peltier technology built-in densitometer. The uncertainty of the density is 2.0×10^{-4} g cm^{-3}.

2.9. Antibacterial activity

Antibacterial tests of the MatILs were carried out using *Staphylococcus aureus*, *Escherichia coli*, *Candida albicans*, and *Cutibacterium acnes*. The broth dilution method was used to evaluate the minimum inhibitory concentration (MIC) of the MatILs. Two-fold dilution ILs (about 100 μL) were prepared and tested in a 96-well microtitre plate. Bacterial strains were cultured in LB broth (Sangon, Shanghai, China) for 15 h at 37 °C, and the fungi in PDB broth (Solarbio, Shanghai, China) for 24 h at 28 °C. A strain suspension at a concentration of 10^6 CFU mL^{-1} was prepared. Next, 100 μL of strain suspension was introduced into wells containing 100 μL of MatILs in dilution series. The bacterial inoculum was obtained and incubated at 28 or 37 °C for 24–72 h, depending on the indicator organism. In the control group, nutrient broth medium was used without ILs. The turbidity was visually assessed, and the lowest concentration at which no bacterial growth was observed compared to the inhibitor-free control was considered to be the MIC value. Three parallel measurements were carried out for each MatIL, and the mean MIC values were obtained.

2.10. Cell toxicity assay

The anticancer activity and cytotoxicity of MatILs were detected by the MTT method, employing two cancer cell lines (HepG2 and A549). In brief, cells were seeded in a 96-well microplate at 8×10^3 cells per well. The cells were treated with different

concentrations of samples for 24 h at 37 °C in a 5% CO_2 environment, followed by removal of the medium. Subsequently, 100 μL of solution containing 0.5 mg per mL MTT was added to each well, and the cells were cultured again for 4 h. The supernatant was discarded, and 100 μL of DMSO was added to each well for dissolution. After gentle shaking for 10 min, the absorbance at 570 nm was measured using an enzyme marker (Tecan Spark 10 M). All tests were conducted in triplicate.

3. Results and discussion

3.1. Characterization of the MatILs

The designed MatILs were synthesized *via* a neutralization reaction by mixing equimolar matrine and a fatty acid, which are two environmentally friendly starting materials derived from biomass. The water content of the MatILs was evaluated by Karl Fischer measurement, and found to not exceed 0.5 wt%. The water content was noted for further calculations.

The chemical structure of the prepared ILs was characterized by NMR, FT-IR, and ESI-MS. The obtained spectral data and spectrograms are shown in Table S1†, Fig. 1 and 2, as well as Fig. S1–S3 of the ESI.† To further confirm the successful synthesis of MatILs, the ^{1}H NMR spectra of MatILs were compared with those of their respective precursor. As an example, Fig. 1 shows the ^{1}H NMR of matrine, *n*-heptanoic acid, and the synthesized [Mat][C$_7$]. The results of ^{1}H NMR revealed that the stoichiometry ratio of heptanoic acid and matrine in ILs was 1 : 1. The –COOH proton peak of *n*-heptanoic acid (11.59 ppm) disappeared in the spectrum of [Mat][C$_7$], and a new peak (7.93 ppm) emerged that corresponded to the protonated amine group. The signals at 2.86, 2.81, and 2.11 ppm produced by the protons attached to C(10), C(2), and C(6) of the matrine molecule shifted to 2.98, 2.93, and 2.20 ppm in [Mat][C$_7$], respectively. This phenomenon confirms the protonation of the N(1) atom because CH$_2$(10), CH$_2$(2), and CH(6) come under the deshielding influence of NH$^+$.

Ionization between the long-chain saturated fatty acid anions and the matrine cation was measured by FT-IR as
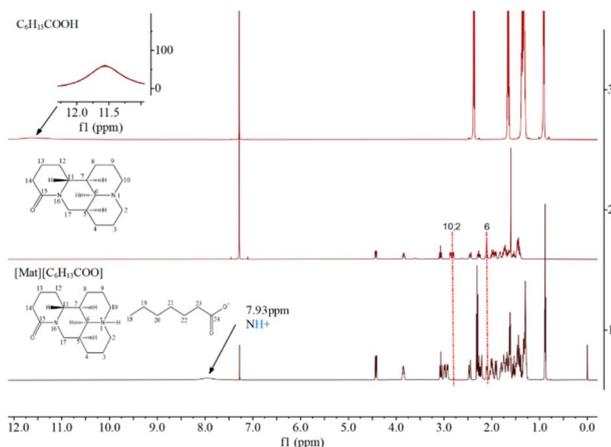

Fig. 1 ^{1}H NMR spectra of matrine, heptanoic acid (C$_6$H$_{13}$COOH), and [Mat][C$_7$].
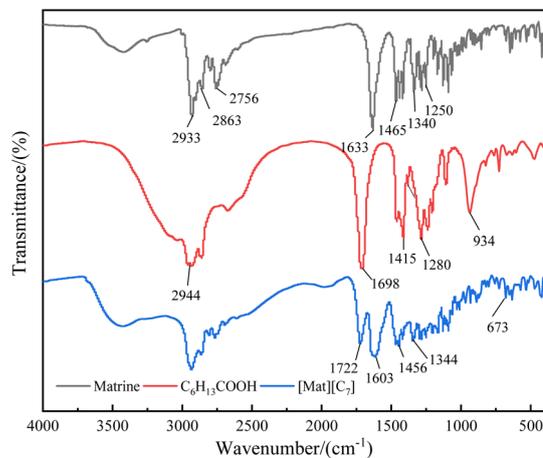

Fig. 2 FT-IR spectra of matrine, heptanoic acid (C$_6$H$_{13}$COOH), and [Mat][C$_7$].

a means of investigating the structural variation of the ILs. The FT-IR spectra of matrine, saturated fatty acids, and ILs are presented in Fig. 2 and S3.† The FT-IR spectrum of matrine shows typical bands of asymmetric and symmetric stretching vibrations, as well as bands of scissoring vibrations from the CH$_2$ group at 2933, 2863, and 1465 cm^{-1}. The characteristic peaks at 2756 and 1340 cm^{-1} were assigned to the stretching and bending vibration of the C–H bond. In addition, 1633 and 1250 cm^{-1} were attributed to the stretching vibrations of the C=O and C–N bonds in the lactam group. The FT-IR plots of heptanoic acid show the C=O and C–O of –COOH characteristic stretching vibration peaks at 1698 and 1280 cm^{-1}, respectively. The signals at 2944, 1415, and 934 cm^{-1} are the stretching, in-plane bending, and out-of-plane bending vibration of the O–H group, respectively.

After the formation of MatILs, the characteristic signals of matrine were also present in the FT-IR spectra of the ILs. Due to the protonation of the nitrogen atoms of matrine, the C=O stretching vibration of lactam at 1633 cm^{-1} shifts to 1603 cm^{-1}. In addition, the absorption bands attributed to the O–H group in fatty acids disappeared in the FT-IR spectra of MatILs. The anti-symmetric and symmetric stretching, as well as the deformation vibration of the carboxylic anions, were observed at 1456, 1344, and 673 cm^{-1}. Furthermore, the bands of stretching vibration of C=O in heptanoic acid shifted to 1722 cm^{-1} from 1698 cm^{-1}, accompanied by a decrease in the peak intensity. These results confirmed the presence of a carboxylic anion. Similar results were observed for the other four MatILs. Then, the formation of matrinium-based ionic liquid was confirmed by NMR and IR data.

3.2. Thermochemical properties of the MatILs

To determine the thermal interaction between matrine cations and fatty acid anions, the thermal behaviour of five MatILs was studied by differential scanning calorimetry (DSC) and thermogravimetric/derivative thermogravimetric analysis (TG/DTGA). The onset decomposition temperature (T_{onset}) was

Table 1 Thermal properties of MatILs

MatILs	T_{onset} (°C)	T_{dmax} (°C)	T_m (°C)	T_g (°C)	$T_{c-c}{}^a$ (°C)
[Mat][C$_7$]	185.5	212.4	−53.08	—	—
[Mat][C$_9$]	196.3	229.2	−56.05	—	—
[Mat][C$_{11}$]	199.4	239.3	−58.21	—	—
[Mat][C$_{13}$]	201.1	246.8	−16.24	−55.37	−37.60
[Mat][C$_{15}$]	271.2	319.4	6.29	−48.33, −26.70	−0.61

^{a} T_{c-c}, cold-crystallization temperature.

estimated from TG curves (Fig. S4†) by the intersection of the starting mass baseline and the tangent line generated through the inflection point. Herein, T_{onset} values of MatILs lay within the range of 185.5–271.2 °C, which indicates their satisfactory thermal stability. The DTG curves show that the decomposition process could be in one or two steps. The temperature corresponding to the maximum exothermic peak in the DTG diagram is expressed as T_{dmax}. The T_{onset} and T_{dmax} of the first decomposition processes are summarized in Table 1.

These results indicate that the thermal stability was enhanced as the length of the anionic alkyl chain increased. This fact may be due to an increase in intermolecular van der Waals interactions. This behavior has already been reported for lauroyl sarcosinate[21] and choline fatty acid salts.[18]

Moreover, DSC was performed to further explore the melting points and/or phase transitions of the MatILs. The DSC curves are given in Fig. S5,† and the obtained melting temperatures (T_m) and glass transition temperatures (T_g) are listed in Table 1. The melting points of all the synthesized compounds are below room temperature, which indicates the nature of ionic liquid. The T_m values along the anionic alkyl series exhibit a V-shaped profile. This phenomenon can be explained by the balance between the decrease in the electrostatic interaction and the regular increase in van der Waals interactions with the increasing anionic alkyl side chain length.[22]

This result has also been previously observed for pyridinium bistriflimide-based ILs[22] and some alkylimidazolium-based ILs.[23] Moreover, the behavior of [Mat][C$_{13}$] and [Mat][C$_{15}$] suggested the occurrence of glass transition, crystallization, and melting processes. The glass transition temperature T_g is an important thermal parameter that provides quite important information regarding intramolecular cohesive energy, and a lower value of T_g indicates lower cohesive energy. The T_g of [Mat][C$_{15}$] in Table 1 is higher than that of [Mat][C$_{13}$]. Cold crystallization and the melting of the crystallites also occur at rather high temperatures for [Mat][C$_{15}$]. The observation of these thermal events showed that a proportion of amorphous material and a crystalline percentage are found in the composition of the two compounds. The presence of a longer alkyl chain in anions of [Mat][C$_{13}$] and [Mat][C$_{15}$] may result in enhanced association and substantial ordering/packing of the molecular ions.

3.3. Solubility and the octanol–water partition coefficient

With the exception of [Mat][C$_{15}$], the other four substances exhibited satisfactory aqueous solubility. Therefore, the solubility of [Mat][C$_{15}$] in water and three buffer solutions and all MatILs in organic solvents were determined, and are given in Tables 2 and S2.† It was discovered that the solubility of [Mat][C$_{15}$] in water is greater than those in the three buffer solutions. The lowest solubility was in SGF (pH 1.2), which indicates that the distribution of [Mat][C$_{15}$] in gastric fluid is worse than that in human body fluid and intestinal fluid. The solubility increased with increasing temperature from 25 °C to 37 °C.

The information regarding the solubility of the drug in organic solvent was helpful not only to strengthen the drug bioavailability and the treatment effect, but also to optimize the pharmaceutical technology and drug dosage form design. Our obtained results are given in Table S2.† None of the MatILs are soluble in petroleum ether, the polarity index of which is the smallest. Except for [Mat][C$_{15}$], the other four MatILs exhibited high solubility in the remaining six solvents. [Mat][C$_{15}$] is soluble in ethyl acetate, dichloromethane, and toluene, while it is insoluble in solvents with a high polarity index (methanol, acetonitrile, and acetone). The excessively long alkyl chain in anion reduced its affinity to the highly polar solvents. This behavior suggests the significant effect of the size of the anionic carbon chain on the miscibility of these MatILs.

The octanol–water partition coefficient ($\log K_{o/w}$) is a critical parameter regarding the lipophilic or hydrophilic properties of a compound, and it can be used to infer the absorption of

Table 2 Saturated solubility (S mol^{-1} dm^{-3}) of [Mat][C$_{15}$] and octanol–water partition coefficient ($\log K_{o/w}$) of MatILs at 25 °C and 37 °C^a

MatILs	pH = 1.2		pH = 6.8		pH = 7.0		pH = 7.4	
	25 °C	37 °C	25 °C	37 °C	25 °C	37 °C	25 °C	37 °C
S (mol dm^{-3})								
[Mat][C$_{15}$]	0.0118	0.0184	0.0168	0.0300	0.0474	0.0942	0.0227	0.0460
Log $K_{o/w}$								
[Mat][C$_7$]	−0.36	0.07	0.01	0.25	0.42	0.69	0.83	1.01
[Mat][C$_9$]	−0.33	0.14	0.02	0.34	0.68	0.81	0.96	1.12
[Mat][C$_{11}$]	−0.32	0.26	0.04	0.35	0.77	0.91	1.20	1.27
[Mat][C$_{13}$]	−0.43	−0.33	−0.07	0.26	0.49	0.65	0.93	0.99
[Mat][C$_{15}$]	−1.17	−1.12	−0.23	0.12	0.46	0.60	0.83	0.93

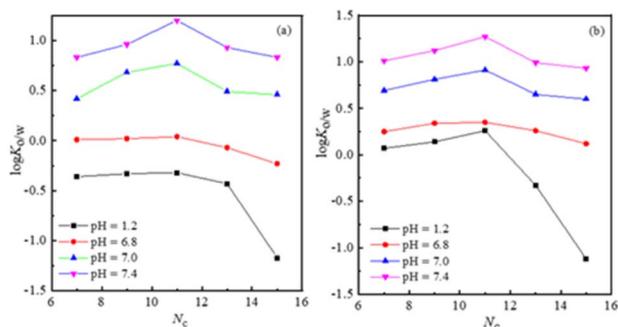^{a} Standard uncertainties u are: $u(T)$ = 0.02 K, $u(S) \leq 0.0001$ mol dm^{-3}.

Fig. 3 The variation of the octanol–water partition coefficient (log $K_{o/w}$) of MatILs with the number of carbon atoms (N_c) of anionic alkyl chain and pH at (a) 25 °C and (b) 37 °C.

a substance in the biological body. Drugs should have a suitable oil–water partition coefficient to accomplish their transfer *in vivo* (water-soluble) and biofilm (fat-soluble) diffusion to the site of binding on the receptor, thus producing drug effects. The most suitable value is $-1 < \log K_{o/w} < 2$.[24] The obtained octanol–water partition coefficients given in Table 2 and Fig. 3 show that nearly all $\log K_{o/w}$ values for matrine and [Mat][C_n] were within the abovementioned range. Furthermore, these values were affected by the pH and temperature of the experimental environment.

The increase in temperature and pH leads to greater liposolubility. The higher $\log K_{o/w}$ values of MatILs in media at 25 and 37 °C and pH 7 and 7.4 indicate that these MatILs were more liposoluble under these media. Furthermore, the $\log K_{o/w}$ increased as the length of the MatILs anionic alkyl chain increased from $n = 7$ to 11, whereas there was no continuous increase in $\log K_{o/w}$ values when $n \geq 13$. For instance, the longest alkyl chain lengths of [Mat][C_{15}] lead to a decrease in $\log K_{o/w}$. This phenomenon may be attributed to excessive aggregation,[24] leading to a weak interaction between IL and *n*-octanol.

3.4. Limited molar conductivity and association constant

A conductivity study of ILs in low concentration regions is significant to better understand the association behavior of an IL in water. The measured conductivities κ of four MatIL aqueous solutions (Tables S3–S6 of the ESI†) were converted to molar conductivities (Λ) and plotted against the square root of MatIL molarity, $c^{1/2}$ in Fig. S6.† Fig. S6† shows that the Λ value of the ILs decays with the rising concentration of MatILs. In high-concentration MatIL solution, ion association, relaxation, and electrophoretic effects occur between the anions and cations of MatILs, leading to additional ion association.

The ionic association constant (K_A) and the limiting molar conductivity (Λ_0) were calculated by the low concentration chemical model (lcCM) according to the following equations:[25]

$$\Lambda = \gamma \left\{ \Lambda_0 \left[1 + C_1(\beta\kappa) + C_2(\beta\kappa)^2 + C_3(\beta\kappa)^3 \right] - \frac{\theta\kappa}{(1 + \kappa R)} \left[1 + C_4(\beta\kappa) + C_5(\beta\kappa)^2 + \frac{\kappa R}{12} \right] \right\} \quad (2)$$

$$K_A = \frac{1 - \gamma}{c\gamma^2 f_{\pm}^2} \quad (3)$$

$$f_{\pm}^2 = \exp[-(\kappa\beta)/(1 + \kappa R)] \quad (4)$$

$$\gamma = \frac{-1 + \sqrt{1 + 4K_A c f_{\pm}^2}}{2K_A c f_{\pm}^2} \quad (5)$$

$$\beta = z^2 e^2 l/(\varepsilon KT) \quad (6)$$

$$\kappa = \left(\frac{8\pi N_A e^2 |Z|^2 \gamma c}{1000 \, \varepsilon\kappa T} \right)^{1/2} \quad (7)$$

$$\theta = |z| \mathrm{Fe}/(299.79 \times 3\pi\eta) \quad (8)$$

where C_i ($i = 1$–5) denotes the function of product ($K_A R$), γ denotes the ionization degree, $f_{\pm}$ denotes an ion activity coefficient, κ and ε represent the Debye coefficient and the permittivity of the solvent, respectively, and R denotes the ion distance parameter. The resulting Λ_0 and K_A values are shown in Table 3. Based on the data presented in Table 3, it is evident that Λ_0 increases and K_A decreases with the rising temperature. The enhancement of temperature leads to a decrease in solvent viscosity, which is beneficial for ionic mobility. However, the increase in temperature is not conducive to ion association.

As expected, the mobility of ions decreases and ionic association improves with increasing length of the anionic alkyl chain. MatILs with anionic alkyl chain length $N_c < 13$ showed low K_A values, inferring a low degree of ionic association in water. A strong ionic association of [Mat][C_{13}] was found, with a 3.00- to 25.2-fold increase in K_A values. Hong *et al.* investigated the effect of the molecular association of ibuprofen-based ionic

Table 3 Limiting molar conductivity (Λ_0), association constant (K_A), distance parameter (R), and standard deviation of fit (σ) for MatILs in water at different temperatures

T (K)	Λ_0 (S cm^2 mol^{-1})	K_A (dm^3 mol^{-1})	σ
[Mat][C$_7$] $R = 0.80$ nm			
298.15	47.78 ± 0.03	6.11 ± 0.61	0.02
303.15	52.96 ± 0.03	3.91 ± 0.48	0.01
308.15	59.37 ± 0.03	1.53 ± 0.37	0.01
[Mat][C$_9$] $R = 0.82$ nm			
298.15	47.11 ± 0.02	6.74 ± 0.44	0.01
303.15	52.90 ± 0.04	4.14 ± 0.68	0.01
308.15	59.10 ± 0.07	1.72 ± 1.03	0.02
[Mat][C$_{11}$] $R = 0.84$ nm			
298.15	44.67 ± 0.06	19.06 ± 1.31	0.01
303.15	49.46 ± 0.06	7.36 ± 1.09	0.01
308.15	55.26 ± 0.07	2.04 ± 1.14	0.01
[Mat][C$_{13}$] $R = 0.86$ nm			
298.15	42.52 ± 0.09	135.22 ± 4.20	0.02
303.15	47.90 ± 0.09	98.09 ± 3.45	0.01
308.15	51.68 ± 0.07	51.48 ± 2.11	0.01

liquid on biological properties and found that higher levels of ionic association were associated with higher lipophilicity, and then more severe cytotoxicity.[26] It is a reasonable speculation that the higher cytotoxicity of [Mat][C$_{13}$] as compared to [Mat][C$_n$] (n = 7, 9, 11) may be related to its larger K_A values (the results of cytotoxicity; see Section 3.8).

3.5. Aggregation behavior of MatILs in water

3.5.1. Electrical conductivity measurement. The assessment of drug micelle formation is important to evaluate its properties and impact on biological processes. The aggregation behavior of four MatILs ([Mat][C$_7$], [Mat][C$_9$], [Mat][C$_{11}$], and [Mat][C$_{13}$]) in aqueous solution at different temperatures was studied by conductivity. The specific conductivity (κ) of MatIL solutions as a function of increasing concentration of MatILs and temperature are listed in Tables S7–S10,† and representative results are displayed in Fig. 4. It is clear that the gradual increase in MatIL concentration leads to two/three readily distinguishable linear dependencies. The curves of [Mat][C$_7$], [Mat][C$_9$], and [Mat][C$_{11}$] show two linear segments whose intersections are designated as cmc. The plot shown in Fig. 4b for [Mat][C$_{13}$] shows three linear regions with different slopes. The relatively low concentration corresponding to the breaking point was assigned to the formation of the premicelle, and is designated as the critical aggregation concentration (cac). Using the method proposed by Aguiar *et al.*, the cmc and cac values were calculated according to the following equation:[27]

$$f(m) = f(0) + \Delta m(A_2 - A_1)\ln[1 + e^{(m-m_0)/\Delta m}]/(1 + e^{-m/\Delta m}) \quad (9)$$

where $f(0)$ denotes the conductivity when the MatIL concentration $m = 0$, and A_1 and A_2 denote the slope of the lower and upper cmc/cac value, respectively. Δm is used to represent the width of an abrupt transition in $f(m)$, and m_0 denotes the concentration of the transition center, corresponding to cmc or cac. The ratio of A_2 and A_1 is usually used to calculate the degree of dissociation (α) of aggregates. The obtained results are listed in Table 4.

The cmc value is mainly determined by the nature of the amphiphile and by the length of its alkyl chain. Fig. 5a shows a plot of the logarithm of cmc *vs.* the carbon atomic number (N_c)

Fig. 4 Specific conductivities *vs.* concentration of (a) [Mat][C$_7$] and (b) [Mat][C$_{13}$] in water at different temperatures.

in the anionic alkyl chain of MatILs. A satisfactory linear plot was observed for [Mat][C$_n$] (n = 7, 9, 11) with a correlation coefficient of 0.9994. Many studies have reported this linear relationship for homologous series of surfactants, known as the empirical Stauff–Klevens rule, as shown in the following formula:[28]

$$\log \text{cmc} = A - BN_C \quad (10)$$

where A and B are constants. The obtained B value is approximately 0.03 and smaller than log 2 (=0.3), and similar values have been obtained for many surface-active materials, such as long chain alkyl imidazolium ionic liquids[29] and amphiphilic quaternary ammonium salts.[30] The small B value signifies that addition of a CH$_2$ group to a hydrocarbon chain was less significant in decreasing the cmc of MatILs. The aggregation of MatILs depends on the length of the anionic chain and also the nature of the counter ion ([Mat]$^+$). For [Mat][C$_{13}$], deviation of the above linear relationship between the log cmc and the alkane chain length was observed (Fig. 5a), suggesting the formation of a premicelle.[31]

Temperature is another important factor affecting cmc. Fig. 5b shows that the cmc values of the four MatILs rise with increasing temperature. This characteristic is consistent with that of typical ionic surfactants. The increased thermal agitation destroys the structural water cage enclosing these hydrophobic moieties, thus enhancing the solubility of the hydrophobic tails.[32] It also delays the formation of micelles, thus increasing the cmc value.

Several thermodynamic parameters are used to understand the thermodynamic behavior of the micellar process. The mass action model is usually utilized to describe the thermodynamic properties of the micellization process in aqueous solution, and the related thermodynamic parameters are computed according to eqn (11)–(13):[33]

$$\Delta G_m^0 = (2 - \alpha)RT \ln X_{\text{cmc}} \quad (11)$$

$$\Delta H_m^0 = -(2 - \alpha)RT^2(\text{d}\ln X_{\text{cmc}}/\text{d}T) \quad (12)$$

$$\Delta S_m^0 = (\Delta H_m^0 - \Delta G_m^0)/T \quad (13)$$

where X_{cmc}, R, and α signify the mole fraction of cmc, gas constant (8.314 J K^{-1} mol^{-1}), and the degree of ionization, respectively. The d ln X_{cmc}/dT value is calculated by fitting ln X_{cmc} to temperature using a second-order polynomial function:

$$\ln X_{\text{cmc}} = a + bT + cT^2 \quad (14)$$

$$\text{d}\ln X_{\text{cmc}}/\text{d}T = b + 2cT \quad (15)$$

where a, b, and c denote regression constants. The obtained thermodynamic parameters are shown in Table 4. It is clear that all ΔG_m^0 values are negative, suggesting that their micellization in water is spontaneous. The ΔG_m^0 values decrease with increasing temperature, signifying that the micellar process was more favorable at higher temperatures. The ΔG_m^0 value becomes more negative as the length of the IL alkyl chain increases. This
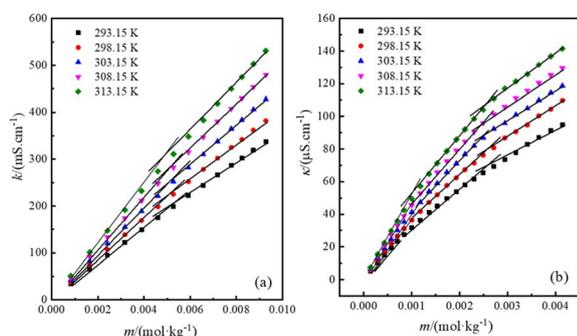
Table 4 The values of cmc/cac, the ionization degree (α), and the thermodynamic parameters of aggregation for MatILs at different temperatures[a]

T (K)	cmc (mol kg^{-1})	α	ΔG_m^0 (kJ mol^{-1})	ΔH_m^0 (kJ mol^{-1})	ΔS_m^0 (J mol^{-1} K^{-1})	$-T\Delta S_m^0$ (kJ mol^{-1})
[Mat][C$_7$]						
293.15	0.00511	0.8986	−24.94	−4.00	71.43	−20.94
298.15	0.00524	0.8976	−25.33	−3.85	72.03	−21.48
303.15	0.00536	0.8989	−25.66	−3.68	72.51	−21.98
308.15	0.00549	0.8927	−26.16	−3.51	73.51	−22.65
313.15	0.00558	0.8987	−26.40	−3.29	73.80	−23.11
[Mat][C$_9$]						
293.15	0.00449	0.8848	−25.61	−3.37	75.88	−22.24
298.15	0.00459	0.8890	−25.89	−3.21	76.06	−22.68
303.15	0.00467	0.8957	−26.12	−3.04	76.13	−23.08
308.15	0.00475	0.8931	−26.56	−2.87	76.88	−23.69
313.15	0.00483	0.8922	−26.97	−2.69	77.53	−24.28
[Mat][C$_{11}$]						
293.15	0.00385	0.8532	−26.77	−4.36	76.44	−22.41
298.15	0.00395	0.8429	−27.39	−3.65	79.65	−23.75
303.15	0.00402	0.8267	−28.19	−2.88	83.51	−25.32
308.15	0.00407	0.8151	−28.90	−2.02	87.26	−26.89
313.15	0.00411	0.7968	−29.80	−1.08	91.70	−28.72
[Mat][C$_{13}$](cac)						
293.15	0.00095	0.7028	−34.70	−3.07	107.89	−31.63
298.15	0.00096	0.7136	−34.97	−2.85	107.74	−32.12
303.15	0.00097	0.7134	−35.49	−2.62	108.42	−32.87
308.15	0.00099	0.7137	−36.04	−2.38	109.21	−33.65
313.15	0.00100	0.7007	−36.96	−2.14	111.17	−34.81
[Mat][C$_{13}$](cmc)						
293.15	0.00235	0.8005	−29.44	−5.10	83.03	−24.34
298.15	0.00240	0.7504	−31.13	−4.67	88.74	−26.46
303.15	0.00248	0.6063	−35.19	−4.44	101.43	−30.75
308.15	0.00251	0.5676	−36.72	−3.70	107.14	−33.01
313.15	0.00255	0.5843	−36.82	−2.75	108.80	−34.07

[a] Standard uncertainties u are: $u(T) = 0.02$ K, u_r(cmc/cac) = 3%, $u(\Delta G_m^0) = 0.03$ kJ mol^{-1}, $u(\Delta H_m^0) = 0.04$ kJ mol^{-1}, $u(\Delta S_m^0) = 0.05$ J mol^{-1} K^{-1}.
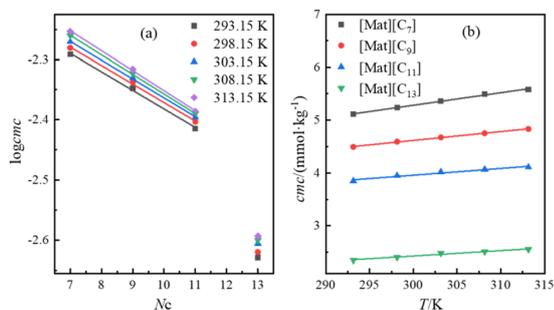
Fig. 5 (a) The linear relationship between the log cmc of MatILs and the number of carbon atoms (N_c) of anionic alkyl chain at different temperatures. (b) The plot of cmc of MatILs with temperature.

occurs because aggregation is more likely to occur with the increase in hydrophobicity.

The negative value of ΔH_m^0 denotes that the micellar process of MatILs is exothermic, which is caused by the binding of antions on the micelle. The positive ΔS_m^0 indicates that during the formation of clusters, the hydration layer around the hydrophobic alkyl chain is destroyed, and additional water molecules are released into the solvent, resulting in increased chaos in the system. As the temperature increases, the values of ΔH_m^0 and ΔS_m^0 increase. The value of $-T\Delta S_m^0$ is much smaller than that of ΔH_m^0, which indicates that the micellar process is entropy-driven over the studied temperature range. With the increase in the length of the MatIL alkyl chain, the $-T\Delta S_m^0$ value becomes more negative, indicating that the hydrophobic effect plays an important part in the micellar process.

3.5.2. Steady-state fluorescence measurement. The aggregation behavior of MatILs was also determined by steady-state fluorescence spectroscopy using pyrene as a fluorescence probe. In the fluorescence spectrum of pyrene solution, the intensity ratio I_1/I_3 of the first (373 nm) and the third (384 nm) vibronic peaks is very sensitive to solvent polarity, and therefore is widely used to measure the polarity of the probe microenvironment[34] and the cmc of surfactants.

Fig. S7† gives the plots of I_1/I_3 values *versus* the MatIL concentrations, and an abrupt sigmoidal decrease was observed. In addition, the I_1/I_3 value for the MatILs decreased

Table 5 Cmc values from different methods and aggregation numbers of MatILs at 298.15 K

| MatILs | cmc (mol kg^{-1}) | | N_{agg} (S_T = 2.5 cmc) |
	Conductivity	Fluorescence	
[Mat][C$_7$]	0.00524	0.00554	25
[Mat][C$_9$]	0.00459	0.00461	64
[Mat][C$_{11}$]	0.00395	0.00384	77
[Mat][C$_{13}$]	0.00240	0.00337	91

with increasing length of the anionic alkyl chain, which reflected the gradual enhancement of the hydrophobic characteristics of the microenvironment[34] and greater ordering at the interface of MatIL micelles. The cmc value was calculated using Boltzmann fitting, and is shown in Table 5. The cmc values obtained by the fluorescence method are equivalent to those obtained from conductivity measurements within the range of common error of different experimental methods.

The mean aggregation number (N_{agg}) was measured by a fluorescence quenching method, in which pyrene was used as a probe, and cetylpyridine chloride (CPC) was used as a quenching molecule. N_{agg} can be computed by utilizing eqn (16):[35]

$$\ln(I_0/I) = \frac{N_{agg}}{S_T - cmc}[Q] \tag{16}$$

where I and I_0 denote the fluorescence intensity of pyrene with and without the quencher CPC, respectively. S_T denotes the total concentration of ILs (=2.5 cmc), and the concentration of CPC is expressed as [Q]. [Q] was varied from 0.2×10^{-4} to 1.0×10^{-4} mol dm^{-3}. The N_{agg} of MatILs in water was determined from the linear relationship between ln (I_0/I) and [Q] (Fig. S8†), and is compiled in Table 5. The determined N_{agg} increases with the increase in the anionic chain length. Similar conclusions were obtained from the investigation of the aggregation number of imidazole ionic liquids.[36] The result shows that aggregation is favored by increased hydrophobicity of the alkyl chain.

3.6. Volumetric properties of the MatILs

Density is one of the most important properties of IL mixtures, and is utilized to predict the thermophysical properties for process design and solution theory. The volumetric properties estimated from density enable us to know the structure and characteristics of the solutions, and this provides significant information regarding ion–ion, ion–solvent, and solvent–solvent interactions as well as the mechanism of bioactive molecules in body systems.

Tables S11–S14† show the experimental density data (ρ) for different molality (m) values of [Mat][C$_n$] (n = 7, 9, 11, 13) over the temperature range of 293.15–308.15 K at 5 K intervals. The density of the [Mat][C$_{15}$] solution was not determined due to its low solubility. Upon careful evaluation of Tables S11–S14,† it can be noted that ρ rises with increasing molality of [Mat][C$_n$] (n = 7, 9, 11, 13) in water and decreases with increasing temperature. Fig. S9† depicts the influence of alkyl chains of [Mat][C$_n$]

on density (taking 293.15 K as an example), and a decreasing trend with the enhancement of N_c was found. This behavior was also observed in aqueous solutions of ILs,[37] amines,[38] and tetraalkylammonium bromides,[39] and may have occurred because as the chain length of the anionic part increases, the non-polar region increases and occupies additional space, resulting in a decrease in total density.

The apparent molar volumes ($V_{2,\varphi}$) of four MatILs in water were calculated based on the density data, using the following equation:

$$V_{2,\varphi} = M/\rho_2 - 10^3(\rho_2 - \rho_1)/m\rho_2\rho_1 \tag{17}$$

where M and m denote the molar mass (g mol^{-1}) and molality (mol kg^{-1}) of MatILs, respectively, and ρ_2 and ρ_1 denote the densities of the binary system ([Mat][C$_n$] + water) and water, respectively. Tables S11–S14† provide the calculated $V_{2,\varphi}$ values for the MatILs in aqueous solution at different temperatures, and the plots of $V_{2,\varphi}$ vs. the molality for the ILs are graphically presented in Fig. S10.†

It was observed that the $V_{2,\varphi}$ value increases with increasing MatIL concentration and temperature. Low concentrations of ILs occupy a small volume in water, which was attributed to the electrostriction effect caused by ionic hydration. With the gradual increase in the solute concentration, the interactions between ions were significantly enhanced, whereas the electrostriction effect of ions on water molecules decreased. This behavior causes the structural water molecules in close proximity to the ILs to be released into the disordered bulk water, and also increases the $V_{2,\varphi}$ value because the structural water molecules are more tightly packed together as compared to the bulk water molecules. Increasing temperature also reduces the interaction between ions and water molecules, thus increasing the total volume.

The apparent molar volume at infinite dilution ($V^0_{2,\varphi}$) of the synthesized MatILs was calculated by the Redlich–Mayer equation, as follows:

$$V_{2,\varphi} = V^0_{2,\varphi} + S_v\sqrt{m} + B_v m \tag{18}$$

where S_v and B_v denote empirical parameters. The obtained $V^0_{2,\varphi}$, S_v, and B_v values are listed in Table 6. Because each ion is surrounded only by solvent molecules at infinite dilution, $V^0_{2,\varphi}$ is not affected by ion–ion interactions, which represent the ion–solvent interaction. The evaluated $V^0_{2,\varphi}$ values are positive, and increase with enhancement of temperature and anion size. This tendency was also found for other types of ILs, such as N-methylcyclohexylammonium-based ionic liquids and guanidinium-based carboxylate ionic liquids.[40] In the IL–water mixed system, the ion–solvent interaction decreases with increasing temperature, and therefore, the $V^0_{2,\varphi}$ value increases.

The result of the enhancement of $V^0_{2,\varphi}$ with anionic alkyl chain principally occurs due to the increased molecular weight of MatILs, hydrophobic interactions, and the making effect of the overall water-structure. The nature of ion–solvent and ion–ion interactions in binary solutions can be understood in terms of S_v parameters. The obtained positive S_v parameters shown in

Table 6 Apparent molar volume at infinite dilution ($V_{2,\varphi}^0$) for aqueous solutions of MatILs, and the parameters S_v and B_v from eqn (18) at different temperatures

T (K)	$V_{2,\varphi}^0$ (cm^3 mol^{-1})	S_v (cm^3 kg$^{1/2}$ mol$^{-3/2}$)	B_v (cm^3 kg mol^{-2})
[Mat][C$_7$]			
293.15	321.56 ± 0.09	17.36	−26.68
298.15	323.31 ± 0.11	15.15	−24.84
303.15	324.72 ± 0.10	10.96	−12.85
308.15	326.82 ± 0.20	3.90	−2.66
[Mat][C$_9$]			
293.15	353.45 ± 0.11	19.54	−30.50
298.15	355.41 ± 0.17	19.41	−30.45
303.15	357.32 ± 0.16	15.03	−14.49
308.15	360.15 ± 0.14	14.83	−21.90
[Mat][C$_{11}$]			
293.15	386.51 ± 0.35	54.68	−48.51
298.15	389.66 ± 0.38	47.27	−35.28
303.15	392.77 ± 0.34	46.04	−44.40
308.15	396.26 ± 0.38	36.41	−29.33
[Mat][C$_{13}$]			
293.15	420.03 ± 0.60	97.79	−171.91
298.15	424.25 ± 0.20	72.82	−115.84
303.15	427.52 ± 0.28	65.87	−106.02
308.15	431.95 ± 0.20	57.01	−97.33

Fig. 6 The apparent molar volume at infinite dilution *vs.* the number of carbon atoms in anionic alkyl chain at different temperatures.
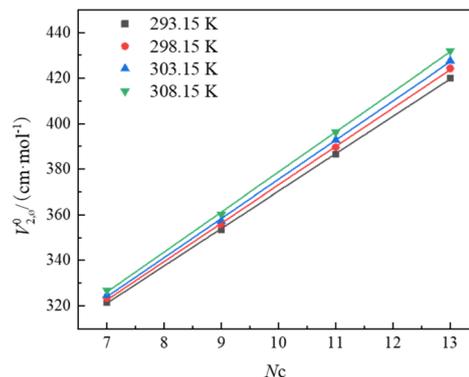
Table 6 indicate that the ion–ion interaction is stronger than the ion–solvent interaction. The negative B_v parameter is due to the existence of a hydrophobic effect and cosphere overlap effects of solute, which increase the ion–ion interaction and the making effect of the water-structure.[41] Moreover, with the increase in the size of anion, positive S_v values increase and B_v becomes more negative, which suggests that more significant ion–ion hydrophobic interactions occur, and it might be due to the more nonpolar nature of longer alkyl chain affecting anion.

The values of $V_{2,\varphi}^0$ for the MatILs were plotted against the alkyl chain length of fatty acid anions in Fig. 6, and a linear relationship was obtained. Therefore, at each temperature, the $V_{2,\varphi}^0$ value can be expressed as:

$$V_{2,\varphi}^0 = V_{mat^+,COO^-}^0 + V_{CH_2}^0 N_c \tag{19}$$

where V_{mat^+,COO^-}^0 represents the sum of $V_{2,\varphi}^0$ of the [Mat]$^+$ and COO$^-$ groups, and $V_{CH_2}^0$ represents the contribution of each CH$_2$ group in the alkyl chain of the fatty acid anion to the $V_{2,\varphi}^0$ of the ILs. The results of fitting to eqn (19) are listed in Table S15,† which shows that the addition of –CH$_2$– groups increased the volume in the range of 16.42–17.58 cm^3 mol^{-1}. The obvious distinction for $V_{CH_2}^0$ was observed in the volumetric properties of different molecules. Millero *et al.*[42] reported the values of 16.1, 15.9, 14.8, 14.1, and 13.8 cm^3 mol^{-1} for $V_{CH_2}^0$ in various compounds. The large values in this work can be interpreted as resulting from bad packing of the –CH$_2$– group into the hydrogen-bonded water networks.

Additionally, the apparent molar expansibility at infinite dilution measures the volume change with temperature, which can be calculated by the differential of eqn (20) with regard to temperature using the following formula:

$$V_{2,\varphi}^0 = k_0 + k_1(T - 273.15) + k_2(T - 273.15)^2 \tag{20}$$

$$E_\varphi^0 = (\partial V_{2,\varphi}^0/\partial T)_p = k_1 + 2k_2(T - 273.15) \tag{21}$$

where k_0, k_1, and k_2 denote coefficients. The calculated E_φ^0 values are listed in Table S16.† As shown in the table, E_φ^0 is positive and increases with increasing temperature and anionic alkyl chain length. This trend may be connected with the enhanced thermal motion caused by the increase in temperature, thus enlarging the solution volume more than that of pure water. However, hydrophobic hydration of ILs increases with rising N_c value, so that the E_φ^0 value becomes more positive as the alkyl chain length increases.

The $(\partial E_\varphi^0/\partial T)_p$ values can be utilized to determine the structural promotion or destructive tendency of the ILs in solution,[43] and were calculated using the following equation:

$$(\partial E_\varphi^0/\partial T)_p = (\partial^2 V_{2,\varphi}^0/\partial^2 T)_p = 2k_2 \tag{22}$$

Table S16† shows that all $(\partial E_\varphi^0/\partial T)_p$ of the MatILs are positive, indicating their structure-making properties in water.[43]

3.7. Antimicrobial activity

The minimum inhibitory concentrations (MICs) for MatILs and matrine is presented in Table 7. The impact of organic anion on biological activity was noticeable. [Mat][C$_7$], [Mat][C$_9$], and [Mat][C$_{11}$] effectively inhibited the growth of the tested bacteria and fungi. The order of antibacterial efficiency was [Mat][C$_{11}$] > [Mat][C$_9$] > [Mat][C$_7$]. This consequence was consistent with the change trend of log $K_{o/w}$ for three MatILs, indicating that the increase in hydrophobicity assists ILs in penetrating the bacterial lipid membrane through hydrophobic–hydrophobic interaction, resulting in cell membrane destruction and finally cell death. However, in the case of [Mat][C$_{13}$] and [Mat][C$_{15}$], no activity was found for four strains.

This phenomenon was also observed in previous studies.[44,45] They found that the antibacterial capacity of ILs did not increase indefinitely with the enhancement of the alkyl chain

Table 7 Bioactivities of matrine and MatILs

	MIC^a (mM)				IC$_{50}$^{b} (mM)	
	E. coli	S. aureus	C. albicans	C. acnes	A549	HepG2
Matrine	50.3	100.7	25.2	50.3	11.75	4.27
[Mat][C$_7$]	33.0	132.1	66.0	66.0	14.05	4.47
[Mat][C$_9$]	30.7	7.7	0.96	3.84	3.15	2.12
[Mat][C$_{11}$]	28.8	0.9	0.46	0.46	0.71	0.45
[Mat][C$_{13}$]	—	—	—	—	0.68	0.30
[Mat][C$_{15}$]	—	—	—	—	0.17	0.15

^{a} Minimum inhibitory concentration ($n = 3$). ^{b} Half-inhibitory concentration ($n = 3$), $P < 0.01$.

length. The MIC value was observed at a certain alkyl chain length rather than the longest alkyl chain length. For example, for pyridinium-based ILs, an alkyl chain length of 12 resulted in the strongest antibacterial activity, and when the alkyl chain length was extended to 14, there was little improvement in the antimicrobial ability. The antimicrobial activity of the higher derivatives of quaternary ammonium salts began to decrease when the alkyl length increased beyond 16. This phenomenon is known as the cut-off effect,[45] and the behaviour should be due to the aggregation of ILs in aqueous solution. The ILs with longer alkyl chains formed micelles at lower concentrations, that is, their surface activity is greater, limiting their diffusion to the cell surface. Compared with matrine, the MIC values of [Mat][C$_9$] and [Mat][C$_{11}$] were smaller, indicating their stronger antimicrobial activity.

Moreover, [Mat][C$_9$] and [Mat][C$_{11}$] exhibited slightly stronger antibacterial effects on Gram-positive bacteria (S. aureus and C. acnes) than on Gram-negative bacteria (E. coli), which may be due to the differences in the bacterial outer membrane. The lipopolysaccharide included in the outer membrane of Gram-negative bacteria reduces their sensitivity to antibiotics.[41]

3.8. Cytotoxicity assay

The cytotoxic effects of matrine and the matrinium-based ILs on two human tumor cell lines (A549 and HepG2) were detected by MTT assay. The semi-inhibitory concentrations (IC$_{50}$) of these ILs are shown in Table 7. It was observed that the IC$_{50}$ values of MatILs (except [Mat][C$_7$]) are less than that of matrine and become smaller with increasing anionic alkyl chain length, which clearly indicates that MatILs with a longer alkyl chain have a greater toxic effect on cells. This result is consistent with published works that discovered that stronger hydrophobicity or long alkyl chains results in high toxicity.[46] A possible reason for this outcome is related to the strong interactions between the lipophilic long alkyl chain of ILs and the plasma cell membrane, leading to membrane rupture and then cell death.

4. Conclusions

Five new matrinium-based API-ILs were prepared using matrine as cations and biodegradable long-chain saturated fatty acid as

anions. The characterization, thermal stability, solubility, and two distinct biological activities were thoroughly investigated. The thermal decomposition temperature of these substances exceeded 185 °C, indicating their excellent thermal stability. The solubility test showed that except for [Mat][C$_{15}$], the solubility in water and the commonly used solvents was satisfactory for the other four matrinium-based ILs.

The antimicrobial influences of [Mat][C$_7$], [Mat][C$_9$], and [Mat][C$_{11}$] on Escherichia coli, Staphylococcus aureus, Candida albicans, and Cutibacterium acnes were significant. The five ILs exhibited cytotoxicity against tumor cells (A549 and HepG2). The association, self-aggregation, and solvation behavior of MatILs in aqueous solution were studied by conductivity, fluorescence, and density methods, respectively. The findings demonstrate that the critical micelle concentration (cmc), limiting molar conductivity (Λ_0), and apparent molar volume at infinite dilution ($V_{2,\varphi}^0$) of MatILs rise with increasing temperature. The process of micelle formation is spontaneous, exothermic, and entropy-driven.

Anionic alkyl chain length is an important factor affecting the studied properties. A growing anionic alkyl chain length is beneficial for ion–ion hydrophobic interactions, the association of ions, and micelle formation. The impact of organic anion on biological activity was also noticeable. MatILs with longer alkyl chains exhibited stronger antimicrobial activity and cytotoxicity, and the activity was improved compared with matrine when the alkyl chain length was longer than 7.

Data availability

The data supporting this article have been included as part of the ESI.†

Author contributions

Conceptualization: Z. Yan, H. Lu; methodology: Z. Yan, M. Xu, H. Lu; investigation: Z. Yan, M. Xu, H. Lu; supervision: Z. Yan, M. Xu; writing – original draft: Z. Yan, M. Xu, H. Lu; writing – review and editing: Z. Yan, M. Xu; funding: Z. Yan.

Conflicts of interest

There are no conflicts to declare.

Acknowledgements

References

1 X. Wu, Q. Zhu, Z. Chen, W. Wu, Y. Lu and J. Qi, Ionic liquids as a useful tool for tailoring active pharmaceutical ingredients, *J. Control. Release*, 2021, **338**, 268–283.

2 P. M. Dean, J. Turanjanin, M. Yoshizawa-Fujita, D. R. Macfarlane and J. L. Scott, Exploring an anti-crystal engineering approach to the preparation of

pharmaceutically active ionic liquids, *Cryst. Growth Des.*, 2009, **9**, 1137–1145.

3 R. M. Moshikur, M. R. Chowdhury, R. Wakabayashi, Y. Tahara, M. Moniruzzaman and M. Goto, Ionic liquids with methotrexate moieties as a potential anticancer prodrug: Synthesis, characterization and solubility evaluation, *J. Mol. Liq.*, 2019, **278**, 226–233.

4 J. M. M. Araújo, C. Florindo, A. B. Pereiro, N. S. M. Vieira, A. A. Matias, C. M. M. Duarte, L. P. N. Rebelo and I. M. Marrucho, Cholinium-based ionic liquids with pharmaceutically active anions, *RSC Adv.*, 2014, **4**, 28126–28132.

5 J. M. Gomes, S. S. Silva and R. L. Reis, Biocompatible ionic liquids: Fundamental behaviours and applications, *Chem. Soc. Rev.*, 2019, **48**, 4317–4335.

6 T. S. de Almeida, A. Julio, N. Saraiva, A. S. Fernandes, M. E. M. Araujo, A. R. Baby, C. Rosado and J. P. Mota, Choline- versus imidazole-based ionic liquids as functional ingredients in topical delivery systems: cytotoxicity, solubility, and skin permeation studies, *Drug Dev. Ind. Pharm.*, 2017, **43**, 1858–1865.

7 D. J. S. Patinha, L. C. Tome, C. Isabel, S. Florindo, H. Soares, A. S. Coroadinha and I. M. Marrucho, New low-toxicity cholinium-based ionic liquids with perfluoroalkanoate anions for aqueous biphasic system implementation, *ACS Sustainable Chem. Eng.*, 2016, **4**, 2670–2679.

8 G. Ren, G. Ding, H. Zhang, H. Wang, Z. Jin, G. Yang, Y. Han, X. Zhang, G. Li and W. Li, Antiviral activity of sophoridine against enterovirus 71 in vitro, *J. Ethnopharmacol.*, 2019, **236**, 124–128.

9 J. Li, S. Wei, D. Marabada, Z. Wang and Q. Huang, Research progress of natural matrine compounds and synthetic matrine derivatives, *Molecules*, 2023, **28**, 5780.

10 A. Adhvaryu, S. Z. Erhan and J. M. Perez, Tribological studies of thermally and chemically modified vegetable oils for use as environmentally friendly lubricants, *Wear*, 2004, **257**, 359–367.

11 A. Willing, Lubricants based on renewable resources-an environmentally compatible alternative to mineral oil products, *Chemosphere*, 2001, **43**, 89–98.

12 A. Jordan and N. Gathergood, Biodegradation of ionic liquids-a critical review, *Chem. Soc. Rev.*, 2015, **44**, 8200–8237.

13 M. U. H. Shah, M. Sivapragasam, M. Moniruzzaman, M. M. R. Talukder, S. B. Yusup and M. Goto, Aggregation behavior and antimicrobial activity of a micellar system of binary ionic liquids, *J. Mol. Liq.*, 2018, **266**, 568–576.

14 A. M. M. Bessa, M. S. C. Venerando, F. X. Feitosa, L. M. A. Silva, F. A. N. Fernandes, R. S. de Santiago-Aguiar and H. B. de Sant'Ana, Low viscosity lactam-based ionic liquids with carboxylate anions: Synthesis, characterization, thermophysical properties and mutualmiscibility of ionic liquid with alcohol, water, and hydrocarbons, *J. Mol. Liq.*, 2020, **313**, 113586.

15 T. L. Greaves and C. J. Drummond, Protic ionic liquids: Evolving structure-property relationships and expanding applications, *Chem. Rev.*, 2015, **115**, 11379–11448.

16 R. M. Pires, H. F. Costa, A. G. M. Ferreira and I. M. A. Fonseca, Viscosity and density of water + ethyl acetate + ethanol mixtures at 298.15 and 318.15 K and atmospheric pressure, *J. Chem. Eng. Data*, 2007, **52**, 1240–1245.

17 M. Hassanpour, S. M. Torabi, D. Afshar, M. H. Kowsari, A. A. Meratan and N. Nikfarjam, Tracing the antibacterial performance of bis-imidazolium-based ionic liquid derivatives, *ACS Appl. Bio Mater.*, 2024, **7**, 1558–1568.

18 M. K. Ali, R. M. Moshikur, R. Wakabayashi, Y. Tahara, M. Moniruzzaman, N. Kamiya and M. Goto, Synthesis and characterization of choline-fatty-acid-based ionic liquids: A new biocompatible surfactant, *J. Colloid Interface Sci.*, 2019, **551**, 72–80.

19 B. S. Furniss, *Vogel's Textbook of Practical Organic Chemistry*, Pearson Education, India, 1989.

20 Y. Wang, J. Chen, Y. Yang, S. Gao, Z. Wang, Y. Liu, X. Zhang, L. Hua, Y. Guo and Y. Yang, Oil–water partition coefficient preparation and detection in the dihydroartemisinin self-emulsifying drug delivery system, *BMC Biotechnol.*, 2022, **22**, 16.

21 N. A. Mustahil, S. H. Baharuddin, A. A. Abdullah, A. Reddy, M. M. Abdul and M. Moniruzzaman, Synthesis, characterization, ecotoxicity and biodegradability evaluations of novel biocompatible surface active lauroyl sarcosinate ionic liquids, *Chemosphere*, 2019, **229**, 349–357.

22 A. I. M. C. Lobo Ferreira, A. S. M. C. Rodrigues, M. Villas, E. Tojo, L. P. N. Rebelo and L. M. N. B. Santos, Crystallization and glass-forming ability of ionic liquids: Novel insights into their thermal behavior, *ACS Sustain. Chem. Eng.*, 2019, **7**, 2989–2997.

23 P. B. P. Serra, F. M. S. Ribeiro, M. A. A. Rocha, M. Fulem, K. Růžička, J. A. P. Coutinho and L. M. N. B. Santos, Solid-liquid equilibrium and heat capacity trend in the alkylimidazolium PF_6 series, *J. Mol. Liq.*, 2017, **248**, 678–687.

24 A. V. Rudraraju, P. N. Amoyaw, T. J. Hubin and M. O. Khan, Determination of log P values of new cyclen based antimalarial drug leads using RP-HPLC, *Pharmazie*, 2014, **69**, 655–662.

25 M. T. Zafarani-Moattar, H. Shekaari and P. Jafari, The role of ionic association of choline amino acid ionic liquids on the two-phase formation and extraction of bovine serum albumin in ATPSs containing PEGDME250 and choline histidine or choline arginine at different temperatures, *Fluid Phase Equilib.*, 2020, **505**, 112352.

26 H. Wu, Z. Deng, B. Zhou, M. Qi, M. Hong and G. Ren, Improved transdermal permeability of ibuprofen by ionic liquid technology: Correlation between counterion structure and the physicochemical and biological properties, *J. Mol. Liq.*, 2019, **283**, 399–409.

27 P. Carpena, J. Aguiar, P. Bernaola-Galván and C. C. Ruiz, Problems associated with the treatment of conductivity−concentration data in surfactant solutions: Simulations and experiments, *Langmuir*, 2002, **18**, 6054–6058.

28 X. Liu, J. Hu, Y. Huang and Y. Fang, Aggregation behavior of surface active dialkylimidazolium ionic liquids [$C_{12}Cnmim$]

Br (n = 1–4) in aqueous solutions, *J. Surfactants Deterg.*, 2013, **16**, 539–546.

29 C. Jungnickel, J. Buczak, J. Ranke, J. F. Fernández, A. Müller and J. Thöming, Micelle formation of imidazolium ionic liquids in aqueous solution, *Colloid Surface A*, 2008, **316**, 278–284.

30 F. Kopecky, Micellization and other associations of amphiphilic antimicrobial quaternary ammonium salts in aqueous solutions, *Pharmazie*, 1996, **51**, 135–144.

31 L. D. Song and M. J. Rosen, Surface properties, micellization, and premicellar aggregation of gemini surfactants with rigid and flexible spacers, *Langmuir*, 1996, **12**, 1149–1153.

32 T. Inoue, H. Ebina, B. Dong and L. Zheng, Electrical conductivity study on micelle formation of long-chain imidazolium ionic liquids in aqueous solution, *J. Colloid Interface Sci.*, 2007, **314**, 236–241.

33 Z. Khan, M. A. Malik, S. A. Al-Thabaiti, A. Alshehri and F. Nabi, Micellization and thermodynamic properties of cationic surfactant cetyltrimethylammonium bromide in non-aqueous mixture of lauric acid, *Int. J. Electrochem. Sci.*, 2017, **12**, 4528–4542.

34 L. Kumar, S. Tanwar, M. K. Banjare, S. Sharma and K. K. Ghosh, Physicochemical studies on the micellization of anionic surfactants in the presence of long alkyl chain ionic liquid, *Chem. Phys. Lett.*, 2021, **769**, 138399.

35 S. E. Burke, S. L. Andrecyk and R. Palepu, Thermodynamic and aggregation properties of sodium dodecyl sulfate in aqueous binary mixtures of isomeric butanediols, *Colloid Polym. Sci.*, 2001, **279**, 131–138.

36 B. Dong, X. Zhao, L. Zheng, J. Zhang, N. Li and T. Inoue, Aggregation behavior of long-chain imidazolium ionic liquids in aqueous solution: Micellization and characterization of micelle microenvironment, *Colloid Surface A*, 2008, **317**, 666–672.

37 R. L. Gardas, D. H. Dagade, S. S. Terdale, J. A. P. Coutinho and K. J. Patil, Acoustic and volumetric properties of aqueous solutions of imidazolium based ionic liquids at 298.15 K, *J. Chem. Thermodyn.*, 2008, **40**, 695–701.

38 M. V. Kaulgud and K. J. Patil, Volumetric and isentropic compressibility behavior of aqueous amine solutions, *J. Phys. Chem.*, 1974, **78**, 714–717.

39 L. H. Blanco and E. F. Vargas, Apparent molar volumes of symetric and asymetric tetraalkylammonium salts in dilute aqueous solutions, *J. Solution Chem.*, 2006, **35**, 21–28.

40 V. Ramkumar and R. L. Gardas, Exploring the solvation behavior of guanidinium based carboxylate ionic liquids in DMSO and DMF through apparent molar properties, *J. Mol. Liq.*, 2021, **343**, 117664.

41 K. R. Patil, V. R. Shaikh, S. K. Patil, D. H. Dagade and K. J. Patil, Thermodynamic studies of aqueous solutions of ammonium based nitrate protic ionic liquids at different temperatures (288.15 K to 303.15 K) and 101.325 kPa: A volumetric approach, *J. Mol. Liq.*, 2019, **287**, 110884.

42 F. J. Millero, A. Lo Surdo and C. Shin, The apparent molal volumes and adiabatic compressibilities of aqueous amino acids at 25 °C, *J. Phys. Chem.*, 1978, **82**, 784–792.

43 D. Singh, G. Sharma and R. L. Gardas, Exploration of the solvation behaviour of ascorbic acid in aqueous solutions of 1,2,4-triazolium based ionic liquid, *J. Mol. Liq.*, 2017, **244**, 55–64.

44 Z. Fang, X. Zheng, L. Li, J. Qi, W. Wu and Y. Lu, Ionic liquids: Emerging antimicrobial agents, *Pharm. Res.*, 2022, **39**, 2391–2404.

45 F. Kopecky, Micellization and other associations of amphiphilic antimicrobial quaternary ammonium salts in aqueous solutions, *Pharmazie*, 1996, **51**, 135–144.

46 R. M. Moshikur, M. R. Chowdhury, R. Wakabayashi, Y. Tahara, M. Moniruzzaman and M. Goto, Characterization and cytotoxicity evaluation of biocompatible amino acid esters used to convert salicylic acid into ionic liquids, *Int. J. Pharm.*, 2018, **546**, 31–38.